Journal of Materials Chemistry

Cite this: J. Mater. Chem., 2011, 21, 19275

www.rsc.org/materials

PAPER

Ionic liquids with fluorinated block-oligomer tails: Influence of self-assembly on transport properties†

Lalitha V. N. R. Ganapatibhotla,[ac] Lin Wu,[a] Jianping Zheng,[bd] Xinli Jia,[a] Dipankar Roy,[b] John B. McLaughlin[a] and Sitaraman Krishnan*[a]

Received 12th September 2011, Accepted 13th October 2011
DOI: 10.1039/c1jm14526f

A novel imidazolium iodide ionic liquid with an ω-perfluoroalkyl poly(ethylene glycol) (PEG) tail attached to the imidazolium ring has been synthesized for its potential incorporation as an electrolyte in dye-sensitized solar cells. The ionic liquid molecules, with block oligomer tails, self-assembled to form a solvent-free ionic gel, without the assistance of an external gelator or an immobilizing matrix. The solidification was evidently facilitated by the generation of ionic clusters due to electrostatic interactions, as well as microphase separation of the immiscible perfluoroalkyl and PEG segments of the cation. We report herein the synthesis and electrochemical properties of this block oligomer ionogel, along with the results of self-consistent mean field calculations probing the formation of nanostructures in the ionogel. Although properties such as high viscosity and high ionic conductivity appear incompatible, it is shown that a nano-structured fluid can support high iodide diffusion at low effective fluidity, and that the formation of an organic alloy, by simple blending of two imidazolium iodide salts, can produce significant conductivity enhancements without lowering the viscosity.

1. Introduction

It is now widely recognized that ionic liquids (ILs) can serve as efficient electrolytes for a variety of electrochemical devices such as dye sensitized solar cells (DSSCs), lithium ion batteries, supercapacitors and fuel cells.[1] The replacement of organic liquid electrolytes by ILs can substantially improve long-term stability and overall device performance by alleviating the problems of vaporization, leakage and component-corrosion that are often linked to conventional electrolytes. For certain devices, particularly the DSSCs, significant efforts in recent years have also been directed at completely avoiding liquid electrolytes by focusing on quasi-solid electrolytes.[2–4]

A major driving force for the activities reported in this area has been the rapid development of high-performance DSSCs with thin-film and flexible structures, where the utility of liquid electrolytes is greatly limited.[5–7] Desorption of dye, corrosion of counter-electrodes, and liquid permeation across the plastic walls of such cells are some of the main issues that can potentially be addressed using quasi-solid gel electrolytes. In contrast to an all-solid high-molar-mass polymer electrolyte, the fluid component of the gel electrolytes facilitates adequate interfacial wetting (of the nanoporous anode). Gel electrolytes, therefore, share the merits of both solid and liquid electrolytes. IL-based gel electrolytes represent a further advancement in this area, where the electrolyte can be imparted with the non-volatile, non-flammable features, as well as the robust electrochemical and thermal stabilities of ILs.[2] However, a challenge in the design of these electrolytes is that the conductivity of an IL is inversely proportional to its viscosity.[8] Consequently, a lowering of the electrolyte fluidity generally adversely affects its ionic conductivity. The present work addresses this last topic, and explores the approach of using microphase separation to forming an ionic gel ("ionogel") electrolyte, wherein the fluidity of the gel can be lowered without substantially compromising its conductivity.

ILs have been gelled by blending with: (1) low molecular weight gelators such as amino acids and sugars, or high molecular weight polymers; (2) inorganic matrices such as carbon nanotubes and silica nanoparticles; and (3) a combination of polymer and inorganic fillers.[1] Benzyl 1-(octadecylcarbamoyl)-2-methylbutylcarbamate,[9,10] cyclohexanecarboxylic acid-[4-(3-tetradecylureido)phenyl]amide,[11] and 1,3:2,4-di-*O*-benzylidine-D-sorbitol and its derivatives[12] have been used as organic gelators in DSSCs. Polymer gel electrolytes, prepared by blending ILs with

[a]*Department of Chemical and Biomolecular Engineering, Clarkson University, Potsdam, New York, 13699, USA. E-mail: skrishna@clarkson.edu; Fax: +1-315-268-6654; Tel: +1-315-268-6661*
[b]*Department of Physics, Clarkson University, Potsdam, New York, 13699, USA*
[c]*Currently at Department of Chemical Engineering, Pennsylvania State University, University Park, Pennsylvania, USA*
[d]*Currently at GLOBALFOUNDRIES, Hopewell Junction, New York, USA*

† Electronic supplementary information (ESI) available: ^{1}H NMR spectrum of ZMeImI; shear stress *vs.* shear rate plots for ZMeImI, ZMeImTf$_2$N, mPEG*n*MeImI, ZOH (Zonyl® FSO-100), and monomethoxy-terminated PEG with an average molecular weight of 550 g mol^{-1} (mPEG12OH); and a schematic of the electrolyte thin film modeled using the SCMF theory. See DOI: 10.1039/c1jm14526f

polymers, have also been widely investigated.[13–18] For example, polymer gel electrolytes have been prepared using 1-propyl-3-methylimidazolium iodide (PrMeImI) IL and poly(vinylidenefluoride-*co*-hexafluoropropylene),[17] poly(ethylene oxide-*co*-propylene oxide),[13] and poly(ethylene oxide).[14,15] Fluoropolymers are good matrices for use in polymer gel electrolytes for DSSCs because of their photochemical stability, even in the presence of TiO_2 and Pt nanoparticles.[17] As an example of hybrid organic–inorganic gel electrolytes, high molecular weight poly(ethylene oxide), poly(vinylidene fluoride), silica fillers, propylene carbonate, 1,2-dimethoxyethane, and LiI have been blended and used in DSSCs.[18] Block copolymers such as polystyrene-*block*-poly(ethylene oxide)-*block*-polystyrene have also been used in polymer gel electrolytes. The triblock copolymer was blended with an IL such as 1-butyl-3-methylimidazolium hexafluorophosphate,[19] and used in the fabrication of polymer thin film transistors.[20]

While multi-component gel electrolytes have been widely studied, there are few published studies on single-component ionogels capable of supporting high ionic conductivities. We report herein ionogel formation from a novel block oligomer IL by spontaneous self-assembly and microphase separation of chemically incompatible moieties in the IL. An imidazolium iodide salt, functionalized with an ω-perfluoroalkyl poly(ethylene glycol) (PEG) group (*cf.* **1**, Fig. 1), was synthesized, and its viscosity, ionic conductivity and morphology were investigated. The IL was a non-glassy, thermoreversible solid, with negligible flow at room temperature (and up to about 80 °C), and may be classified as an ionogel[1] because, as will be shown using self-consistent mean field theory simulations, it consisted of fluid-like ion-conducting PEG nanochannels interspersed with fluorinated immobilizing domains. No gelator, either low molecular weight or polymeric, was required for fluidity reduction. In contrast, PEGylated ILs of comparable molecular weights, but without the perfluoroalkyl groups in the IL tails (**2**, Fig. 1), and the block oligomer imidazolium IL with bistriflimide anion (Tf_2N, **1b**, Fig. 1) were relatively low-viscosity liquids. In this article, the transport properties of the new fluorinated imidazolium iodide ionogel, **1a**, will be compared with those of the imidazolium ILs **1b** and **2**. An approach of alloying the ionogel with a crystalline solid, **3** (Fig.1), to obtain conductivity enhancements will also be presented.

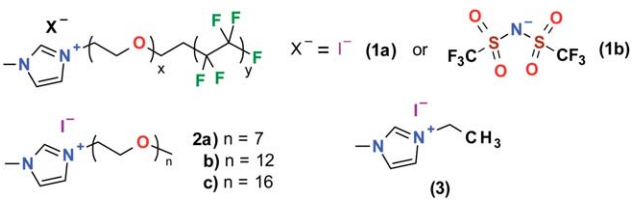

Fig. 1 Chemical structures of ω-perfluoroalkyl PEG functionalized imidazolium iodide IL (**1a**, denoted by ZMeImI) and ω-perfluoroalkyl PEG functionalized imidazolium bistriflimide IL (**1b**, denoted by ZMeImTf$_2$N), and of the ω-methoxy PEG functionalized imidazolium iodide ILs (**2**, mPEG*n*MeImI) and 1-ethyl-3-methylimidazolium iodide (**3**, EtMeImI) that have been reported previously.[21] The average values of x and y in the block oligomer ILs, **1**, are about 6.5 ± 0.5 and 3.5 ± 0.5, respectively.

2. Experimental section

2.1. Materials

1-Methylimidazole (CAS no. 616-47-7, Aldrich, Milwaukee, WI, 99%), ω-perfluoroalkyl poly(ethylene glycol) (Zonyl® FSO-100, $F(CF_2CF_2)_y(CH_2CH_2O)_xCH_2CH_2OH$, CAS no. 65545-80-4, Aldrich), *p*-toluenesulfonyl chloride (TsCl, CAS no. 98-59-9, Acros Organics, Morris Plains, NJ, >99%), anhyd. sodium iodide (CAS no. 7681-82-5, Aldrich, 99.999%), iodoethane (CAS no. 75-03-6, Sigma-Aldrich, Milwaukee, WI, 99%), and silver nitrate (CAS no. 7761-88-8, Sigma-Aldrich, >99.8%) were used as received. Anhyd. pyridine, methylene chloride, acetone, *N*,*N*-dimethylformamide (DMF), sodium bicarbonate, hydrochloric acid, sodium thiosulfate, anhyd. sodium sulfate, diethyl ether (Et_2O), and lithium bis(trifluoromethylsulfonyl)amide ($LiTf_2N$, CAS no. 90076-65-6, Oakwood Products, West Columbia, SC, 99%) were also used as received. Solvents for reaction were dried using Type 3 Å molecular sieves (Sigma-Aldrich).

2.2. Synthesis of ω-perfluoroalkyl PEG functionalized imidazolium block oligomer ILs

A three-step procedure was used for the synthesis of ZMeImI (*cf.* Scheme 1).

Tosylation of ω-perfluoroalkyl PEG (ZOH). ZOH (50 g, 69.1 mmol) was mixed with anhyd. pyridine (8.19 g, 103.5 mmol) in a round-bottom flask, and a solution of TsCl (19.72 g, 103.4 mmol) in anhyd. CH_2Cl_2 (100 mL) was added dropwise to the flask while cooking the flask in an ice bath (~0 °C). The addition of TsCl was accompanied by the formation of a white precipitate. After 1 h, the reaction mixture was warmed back to room temperature. After 24 h of mixing at room temperature, CH_2Cl_2 (100 mL) was added to the reaction flask and the resulting mixture was stirred for 30 min, followed by sequential extractions with satd. $NaHCO_3$ soln. (3 × 50 mL), 1 M HCl soln. (3 × 50 mL), and distilled water (3 × 50 mL). The organic phase was dried over sodium sulfate, filtered, and concentrated by evaporation of CH_2Cl_2 under vacuum. The resulting yellow liquid was dried at 50 °C overnight, and was found (using the relative areas of the CH_2OTs and CH_2CF_2 peaks in the ^1H NMR spectrum) to contain 84 mol % ZOTs and 16 mol % ZOH. About 47 g of the crude product was obtained, which was used in the next step without further separation. The molar yield of ZOTs was about 67%. δ_H (400 MHz; $CDCl_3$; Me_4Si) 7.79 and 7.34 (dd, $J = 8.3$ Hz,

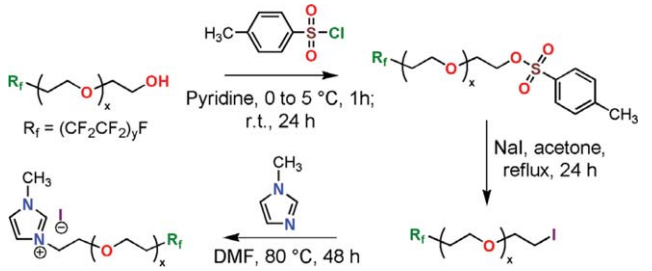

Scheme 1 Synthesis of methylimidazolium ionic liquid with perfluoroalkyl-terminated poly(ethylene glycol) tail.

4H, aryl ring), 4.16 (t, $J = 4.8$ Hz, 2H, CH_2OTs), 3.86–3.51 (m, CH_2CH_2O, 29.1H), 2.53–2.31 (m, 5.4H, ArCH_3 and CH_2CF_2).

Iodination of ZOTs. NaI (27.28 g, 182 mmol) was added in the dark, with vigorous stirring, to crude ZOTs (44.26 g, 43.6 mmol ZOTs) dissolved in acetone (140 mL), and the resulting pale yellow mixture was stirred under reflux (at about 60 °C). A yellow precipitate eventually settled down in the flask. After evaporating acetone using a rotary evaporator, CH_2Cl_2 (100 mL) and distd. water (80 mL) were added to the precipitate. The mixture was stirred well for 30 min, and the organic and aqueous phases were separated using a separatory funnel. The organic phase was extracted with 5% aq. $Na_2S_2O_3$ solution (3 × 50 mL). The organic phase was further washed with satd. $NaHCO_3$ soln. (3 × 50 mL), and with distd. water (3 × 50 mL), and dried over sodium sulfate. The sodium sulfate was removed by filtration, and the clear yellow solution was concentrated under vacuum. The product was further dried in a vacuum oven at 50 °C to obtain ZI as a viscous yellow liquid (32 g). The yield of the product, which was almost pure ZI (based upon the relative areas of the CH_2I and CH_2CF_2 peaks in the ^{1}H NMR spectrum), was 88%. δ_H (400 MHz; $CDCl_3$; Me_4Si) 3.56–3.76 (br m, 26.7H, CH_2CH_2O), 3.27 (t, $J = 6.9$ Hz, 2H, CH_2I), 2.54–2.33 (m, 2H, CH_2CF_2).

Quaternization of 1-methylimidazole with ZI. 1-Methyl imidazole (6.10 g, 74.3 mmol) was added to a round-bottom flask containing ZI (31 g, 37.2 mmol) and DMF (10 mL) and the mixture was stirred at 80 °C under nitrogen for 48 h. After cooling to room temperature, the reaction mixture was added slowly to cold (~0 °C) Et_2O with vigorous stirring, which resulted in phase separation of the product. The top Et_2O layer was decanted off, and the product was repeatedly washed with fresh Et_2O, after which it was dried in a vacuum oven at 50 °C for about 12 h. The yield of ZMeImI was about 25 g (molar yield of about 73%). The absence of ZOH or ZI impurity in the product was confirmed using the ratio of experimental areas under the NCH_3 and CH_2CF_2 peaks in the ^{1}H NMR spectrum, which was fairly close to the stoichiometric value of 1.5 (*cf.* ESI†). δ_H (400 MHz; $CDCl_3$; Me_4Si) 10.43–9.76 (m, N^+CHN), 7.89–7.10 (m, NC*H* and N^+CH), 4.59 (t, $J = 4$ Hz, 2H, N^+CH_2), 4.04 (s, 3H, NCH_3), 3.93 (t, $J = 4.4$ Hz, 2H, $N^+CH_2CH_2O$), 3.84–3.50 (br s, 23H, CH_2CH_2O), 2.49–2.32 (br m, 2H, CH_2CF_2).

Anion metathesis reaction. ZMeImTf_2N was prepared by a metathesis reaction on ZMeImI using LiTf_2N. An aq. soln. of LiTf_2N (25 wt%, 5.7 g, 5 mmol LiTf_2N) was added dropwise to an aq. soln. of ZMeImI (25 wt%, 12 g, 3.3 mmol ZMeImI) with vigorous stirring at room temperature, which resulted in an instantaneous formation of a turbid mixture. The stirring was stopped after 12 h. The mixture separated into two distinct layers within 1 h of stopping the stirrer. The top aq. phase was decanted off, and the IL was thoroughly extracted using distilled water (5 × 15 mL) such that any further washing did not result in a precipitate with aq. $AgNO_3$ soln. (10 wt%) (indicating the absence of iodide in the extract). The resulting IL was dried in a vacuum oven at 50 °C for 24 h. Yield 3.1 g (88%).

The ω-methoxy PEG functionalized imidazolium iodides (mPEG*n*MeImI) and 1-ethyl-3-methylimidazolium iodide (EtMeImI) were synthesized as reported previously.[21]

2.3. Formation of blends of ZMeImI and EtMeImI, and ZMeImI and LiI

Blends of ZMeImI and EtMeImI were prepared by stirring a solution of both the iodides in acetone for about 12 h, followed by evaporation of acetone using a rotary evaporator and a vacuum oven. Blends of ZMeImI and EtMeImI with EtMeImI mole fractions, $x_E = 0.09$, 0.25, 0.50, 0.56, 0.63, and 0.75 were prepared and analyzed using differential scanning calorimetry (DSC). Similarly, blends of ZMeImI with LiI, with LiI mole fractions, $x_{LiI} = 0.09$ and 0.50, were prepared and analyzed.

2.4. Physicochemical characterization

NMR spectroscopy, thermogravimetry (TG), DSC, viscometry, and electrochemical impedance spectroscopy (EIS) of the ILs were performed using previously published procedures.[21] Before analysis, the samples were thoroughly dried for 24 h at 50 °C *in vacuo*. A Bruker Avance 400 MHz NMR spectrometer was used to record the ^{1}H NMR spectra in anhyd. deuterated chloroform (99.8 atom % D, 0.03% v/v tetramethyl silane, TMS), and chemical shifts were determined relative to TMS. Thermogravimetric analysis was conducted using a Perkin-Elmer Pyris 1 Thermogravimetric Analyzer. The sample was heated in a Pt pan under nitrogen purge, over a temperature range of 40–600 °C, at a rate of 15 °C min^{-1}. A Brookfield LVDV-II + Pro model cone and plate viscometer, equipped with a model CP 52 cone spindle (operating range of 4.6 to 9.2 × 10^4 cP) was used for viscosity measurements. The sample holder of the viscometer was sealed with a Teflon tape to prevent moisture uptake by the sample during measurement. The viscosity of ZMeImI was determined at temperatures of 85, 90, and 95 °C. The viscosities at lower temperatures were higher than the upper limit of the measurement range of the instrument. At each temperature, the viscosity was determined using different rotational speeds of the spindle, to characterize the viscosity *vs.* shear rate behavior. Aluminum pans with pin-holes in the lids, for *in situ* drying of samples, were used for DSC measurements (carried out in a nitrogen atmosphere using TA Instruments Q100 Differential Scanning Calorimeter). Temperature calibration was performed using the onset temperature of the melting of indium at 156.6 °C. The sample temperature was ramped to 100 °C, held at this value for 10 min, decreased to −80 °C at a rate of 2 °C min^{-1}, held at −80 °C for 2 min, and increased again to 100 °C at a rate of 20 °C min^{-1}. Data reported herein are those obtained during the second heating step.

Ionic conductivities were determined as a function of temperature using electrochemical impedance spectroscopy (EIS).[21] To fill the test cell with the ionogel, the fluidity of the gel was increased by heating it to a temperature >90 °C. The cell consisted of two identical flat electrodes of stainless steel in a Teflon housing, and was placed in a TESTEQUITY 105A environmental chamber for temperature control. Activated silica gel was placed in this chamber to minimize moisture absorption by the sample during conductivity measurements. The cell

constant, determined from standard KCl solution, was found to be 0.24 cm^{-1}. EIS data were recorded as Nyquist plots with 15 mV amplitude A.C. perturbation voltages at different frequencies between 3 Hz and 300 kHz. Experimental Nyquist spectra were validated through Kramers–Kronig (KK) transform procedures, and analyzed using complex nonlinear least square (CNLS) technique to determine the appropriate electrode equivalent circuit (EEC) model for evaluating the bulk resistance, and hence the conductivity of the electrolyte.

2.5. Self-consistent field simulations

Microphase separation in the ionogels was studied using the self-consistent mean field (SCMF) model developed by Scheutjens and Fleer.[22,23] Numerical calculations were implemented using *sfbox* software developed at Wageningen University.[24] Simulations were carried out for both pure ZMeImI, and its blends with EtMeImI. The effects of the ratio of the two components in the blends, the polydispersity in the perfluoroalkyl-terminated PEG tails, and simulation variables such as interaction parameters and coordination number were investigated. The Flory–Huggins interaction parameter between CF_2 and CH_2CH_2O was estimated[25] to be about 1.3, using the solubility parameters of polytetrafluoroethylene and PEO (12.7 and 22 $MPa^{0.5}$, respectively), and using an average volume of lattice cell equal to 60 $Å^3$. The interaction parameters were assumed to be 0 for CH_2CH_2O and the imidazolium cation, and for CH_2CH_2O and iodide. Additional simulations were performed with other choices for the interaction parameters, and it was found that the results were relatively insensitive to the values that were used. The Poisson equation was used to model electrostatic potentials, and the local relative permittivity was calculated as a sum of the relative permittivities of the constituent mers, weighted by the local volume fractions of these mers.[26] Periodic boundary conditions were used for the two sides perpendicular to the electrolyte-vacuum interface, and a reflecting boundary condition was used at the fourth side, parallel to the interface.

3. Results and discussion

3.1. Thermogravimetric analysis

Fig. 2 shows the TG results for ZMeImI. It is seen that the IL is stable up to a temperature of about 225 °C. The temperature corresponding to 5% mass loss is about 266 °C, which is lower than the corresponding temperature (281 °C) for the non-fluorinated IL, mPEG7MeImI.[21] The rate of mass loss ($-dm/dT$) is maximum at the temperatures of 328 and 331 °C for ZMeImI and mPEG7MeImI, respectively.

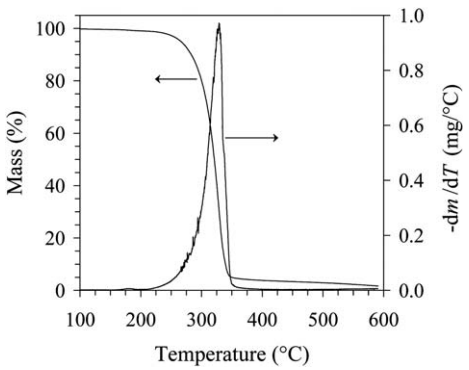

Fig. 2 TG of ZMeImI at 15 °C min^{-1} in a nitrogen atmosphere.

3.2. Viscosity measurements

ZMeImI is a *hard-gel*[27] at 25 °C, that is, it does not flow out of an inverted tube at this temperature (*cf.* Fig. 3). Its viscosity could not be determined (with the instrument used) below a temperature of about 85 °C. The mechanisms responsible for the rather low fluidity of ZMeImI could include various effects of molecular weight,[28] tail length,[21] as well as microstructure formation (microphase separation) in the fluid.[29–31] To explore the first two possibilities, the viscosities of ZMeImI were measured at 85–95 °C, where the sample attained a more fluid state to permit such measurements. The results were then compared with the liquid phase viscosities, measured at the same temperatures, for another group of PEGylated ILs (*cf.* **2**, Fig. 1) that had molecular weights and chain lengths comparable to those of ZMeImI.

Fig. 4 shows the viscosity of ZMeImI as a function of shear rate, at temperatures of 85, 90 and 95 °C. A shear-thinning (pseudoplastic) behavior was observed. The non-fluorinated mPEG*n*MeImI ILs, **2** (Fig. 1), on the other hand, were Newtonian liquids with a shear-independent viscosity[21] (see electronic supplementary information (ESI) for shear stress *vs.* shear rate plots).

Table 1 compares the zero-shear-rate viscosities of ZMeImI at 85 and 95 °C (extracted from a least-square fit of the experimental viscosity *vs.* shear-rate data to the Powell–Eyring model[32]), with the viscosities of ZMeImTf_2N and the mPEG*n*-MeImI ILs at these temperatures. Also shown in this table are a comparison of the sizes of the molecules, in terms of molecular weights, and a comparison of the tail lengths, in terms of the numbers of atoms along the backbone of the tail. It is seen that the viscosities of ZMeImI are disproportionately higher than those of the mPEG*n*MeImI ILs, although the molecular weights and tail lengths of the two types of ILs are similar.

We attribute the low fluidity of ZMeImI to the microstructured nature of this IL. Microstructure formation evidently occurs because of the immiscibility of fluoroalkyl segments with the PEG segments and the ionic groups in the IL, and the formation of ionic clusters that bridge the chain ends and create a transient network.[33,34] Because there were no covalent cross-links, gelation in ZMeImI was thermoreversible, that is, ZMeImI could be reversibly transformed from a solid state at room temperature to a fluid state at temperatures above 85 °C. The

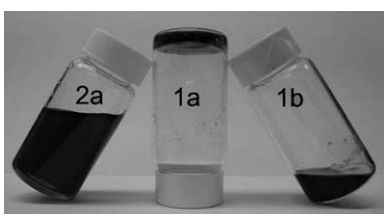

Fig. 3 A photograph of ILs **2** and **1**, with homopolymer and block oligomer tails, respectively. Ionogel 1a, shown in the inverted vial, does not flow at room temperature.

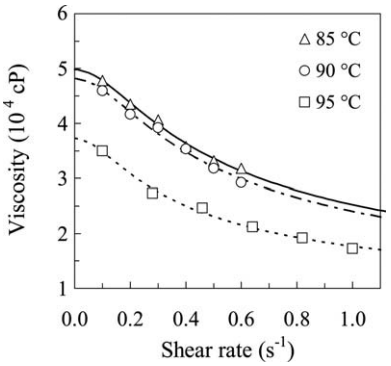

Fig. 4 Temperature dependence of the shear thinning (non-Newtonian) viscosity of ZMeImI. The lines represent the Powell–Eyring fit.

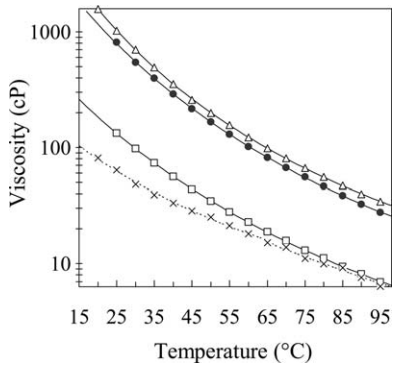

Fig. 5 Temperature dependence of viscosities of mPEG12MeImI (△), $ZMeImTf_2N$ (●), and ZOH (□), and $CH_3(OCH_2CH_2)_{12}OH$ (×). The solid lines represent VFT fits. Data for mPEG12MeImI are re-plotted from ref. 21.

increase in fluidity at higher temperatures is due to a relatively low glass transition temperature of the IL (*cf.* section 3.4), and due to the weakening of van der Waals and electrostatic interactions at higher temperatures. The importance of ionic interactions in viscosity enhancement is evident from the fact that the viscosities of ZMeImI were much higher than those of the analogous $ZMeImTf_2N$ block oligomer IL with the Tf_2N anion. Electrostatic interactions are expected to be weaker with the larger Tf_2N anion (than iodide) because of charge delocalization. Moreover, the nonionic ω-perfluoroalkyl PEG (ZOH) precursor was, in fact, found to have rather low viscosities of about 9.4 and 6.9 at 85 and 95 °C, respectively. The microphase separation in ZMeImI was confirmed using a self-consistent mean-field (SCMF) lattice simulation, as discussed in section 3.5.

Both ion-cluster formation and microphase separation of the perfluoroalkyl and PEG segments contributed to the viscosity enhancement in the block-oligomer IL. The mPEG*n*MeImI ILs are also monochelic ionomers, similar to ZMeImI, but have lower viscosity because of the absence of the fluoroalkyl microdomains. Furthermore, ionic aggregation is difficult in mPEG*n*MeImI because of the somewhat high relative permittivity, ε, of PEG ($\varepsilon = 7.68$ for tetraethylene glycol dimethyl ether), whereas ion-cluster formation is facilitated in ZMeImI because of the lower permittivity of perfluoroalkanes ($\varepsilon = 1.76$ for perfluorohexane). Similarly, ionic aggregation is less likely in the case of the bulky, charge-delocalized bistriflimide anion, so that its viscosity is similar to those of the mPEG*n*MeImI ILs (*cf.* Fig. 5). The slightly lower viscosity of $ZMeImTf_2N$ can be attributed to the weaker intermolecular forces of interaction due to the non-polar perfluoroalkyl groups, and to the partial miscibility of the bistriflimide anion with the fluoroalkyl segments of the IL tails that would affect microphase separation.

The role of microphase separation in viscosity enhancement is evident by comparing the viscosities of ω-perfluoroalkyl PEG (ZOH) and ω-methoxy PEG (mPEG*n*OH), the precursors of ZMeImI and mPEG*n*MeImI ILs, respectively. Fig. 5 shows the viscosities of ZOH and $CH_3(OCH_2CH_2)_{12}OH$ at different temperatures. The two precursors have approximately the same number of atoms along the chain backbones. ZOH is expected to undergo microphase separation (from SCMF simulations), whereas mPEG12OH is a homogeneous fluid. ZOH was found to have a higher viscosity, especially at lower temperatures, compared to mPEG12OH, in spite of its non-polar fluoroalkyl constituent. In summary, the low fluidity of ZMeImI is attributable to ionic aggregation at one end and perfluoroalkyl aggregation at the other end of the block-oligomer molecules. The ionic gel did not form if any one of these aggregations was absent.

3.3. Impedance spectroscopic measurement of ionic conductivity

Fig. 6 shows an illustrative selection of raw EIS data (in the form of Nyquist plots) that were used to determine the temperature-dependent ionic conductivities. The symbols denote experimental results and the lines show CNLS fits to the data using the EEC shown in the inset of Fig. 6. Apart from providing the necessary framework for conductivity calculations, the EEC elements also model the overall electrical-response characteristics of the

Table 1 Comparison of viscosities of imidazolium ILs with block oligomer and homopolymer tails

IL	Mol. wt. (g mol^{-1})	No. of atoms along the tail backbone	Viscosity (cP)	
			85 °C	95 °C
ZMeImI (**1a**)[a]	916	31	49 800	37 200
$ZMeImTf_2N$ (**1b**)	1068	31	38.5	27.7
mPEG7MeImI (**2a**)[b]	532	22	40.6	29.0
mPEG12MeImI (**2b**)[b]	753	37	47.1	34.2
mPEG16MeImI (**2c**)[b]	929	49	49.3	35.8

[a] Zero-shear-rate viscosity extracted from the Powell–Eyring fit. [b] Data from ref. 21.

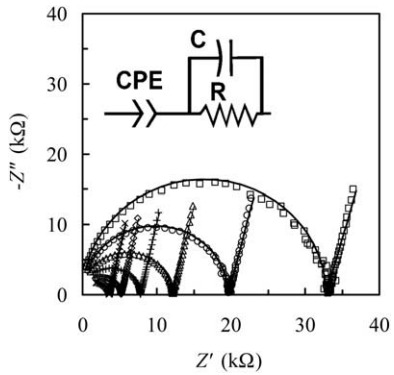

Fig. 6 Complex impedance plots for the ZMeImI acquired at temperatures $T = 20$ °C (□), 25 °C (○), 30 °C (△), 35 °C (+), 40 °C (◇), and 45 °C (×).

electrolytes in the two-electrode environment of a standard conductivity cell.

The Nyquist plots in Fig. 6 are typical of Faradaically blocking electrodes in contact with polymer electrolytes. The left and right ends of the Z' axis correspond to data points obtained at the high and low frequency extremes, respectively, of the impedance spectra. The constant phase element (CPE) represents the frequency-dispersed capacitive attribute of the Faradaically blocking electrodes,[35,36] which is commonly observed in EIS-based measurements of polymer conductivities. The *R*-*C* unit of the EEC represents the bulk electrolyte, with *R* and *C* denoting the electrolyte resistance and the net cell capacitance, respectively. The total complex impedance (Z) of this EEC has the form $Z = Z' + jZ'' = Z_Q + Z_b$, where Z_Q and Z_b are the impedance contributions of the CPE and the bulk electrolyte, respectively. The CPE impedance is written as $Z_Q = Z_Q' + jZ_Q'' = a/(j\omega)^{\alpha}$. Here, a and α are frequency independent CPE parameters,[31] ω denotes the perturbation frequency of EIS, and $j = (-1)^{1/2}$. Therefore, $Z_Q' = (a/\omega^{\alpha})\cos(\alpha\pi/2)$ and $Z_Q'' = -(a/\omega^{\alpha})\sin(\alpha\pi/2)$. The value of the CPE index α ($0 \leq \alpha \leq 1$) is a measure of the interfacial roughness and spatial inhomogeneity. $\alpha = 1$ corresponds to a flat capacitive interface. The impedance components for the electrolyte are $Z_b' = R/[1 + (\omega RC)^2]$ and $Z_b'' = -\omega R^2 C/[1 + (\omega RC)^2]$. The relative effects of the electrode–electrolyte interface (CPE) and the bulk electrolyte (*R*-*C* combination) on the EIS data can be analyzed as follows, using these analytical expressions for Z_Q and Z_b.

In the lowest frequency region, Z_Q' and Z_Q'' dominate the Nyquist spectra, and result in slanted straight lines of the functional form $Z_Q'' = -Z_Q'\tan(\alpha\pi/2)$.[35] The slopes of the lines depend on the value of α. In the intermediate low-frequency regime, $Z_b' \rightarrow R$ and $Z_b'' \rightarrow 0$. At very high frequencies, both Z_b' and Z_b'' approach zero. Thus, the semi-circular arcs in the mid to high frequency range of the Nyquist spectra in Fig. 6 are governed by the *R*-*C* unit of the EEC. The points of intersection of the low frequency ends of the semicircles with the Z' axis provide the values of *R*. At these points, $Z_Q'' = Z_Q' = 0$, $Z'' = 0$, and $Z' = R$. As the sample temperature is increased, the Nyquist plot progressively shrinks to reflect the corresponding decrements in the net interfacial impedance, and the point corresponding to the condition $Z' = R$ also shifts to lower values. In the present study, CNLS analysis was used for accurate evaluation of *R* as well as of the other EEC elements.

The CNLS-derived values of α were mostly confined between 0.80 and 0.86 throughout the temperature range explored in the EIS experiments. These values of α (reasonably close to 1) are representative of a uniform distribution of the ZMeImI electrolyte at the electrode interfaces. Microscopic roughness of the electrode surfaces is most likely responsible for restricting α to a value that was slightly below 1. The admittance amplitude of the CPE, measured in terms of the parameter $1/a$, gradually increased from 6 to 25 μF $s^{\alpha-1}$, as the cell temperature increased from 0 to 110 °C. This indicated a measurable increase in the effective electrode–electrolyte contact area with increasing temperatures. The value of C in a typical blocking-electrode conductivity cell is largely controlled by the geometric cell-capacitance, and hence by the electrode configuration.[37] Consistent with this description, C remained in the nF regime, essentially independent of the applied temperature variations.

The temperature dependent resistance *R* serves as the most relevant EIS parameter in the present context. The conductivity, λ, of the test sample was determined in terms of this resistance using $\lambda = k/R$, where k is the cell constant. These conductivity data for ZMeImI are presented in Fig. 7 for temperatures in the range of 0 to 110 °C. Ionic conductivities measured for mPEG16MeImI under similar experimental conditions also are included here for comparison. Both sets of data could be described well by the Vogel–Fulcher–Tammann equation $\lambda = \lambda_0\exp\{-C/(T-T_0)\}$, where λ (mS cm^{-1}) is the conductivity, T/K is the absolute temperature, and λ_0 (mS cm^{-1}), T_0 (K), and C (K) are the parameters of the VFT equation. The values of λ_0, T_0, and C are 167.69 mS cm^{-1}, 206.36 K, and 872.59 K, respectively, for ZMeImI, and 249.49 mS cm^{-1}, 188.03 K, and 844.45 K, respectively, for mPEG16MeImI.

The conductivities of the PEGylated imidazolium iodide ILs have been found to conform to the Nernst–Einstein equation, which predicts that the conductivity is inversely proportional to viscosity.[21] From Table 1, it is seen that the viscosities of ZMeImI at 85 and 95 °C are about 1000 times higher than those of mPEG16MeImI. However, the conductivities at these temperatures are only about 3 times lower than those of mPEG16MeImI (*cf.* Fig. 7 and Table 2). The relatively high conductivity of ZMeImI, in spite of its high viscosity, is attributed to microphase separation of the PEG and fluoroalkyl segments forming

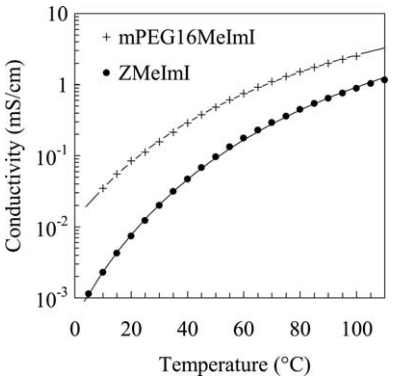

Fig. 7 Temperature dependence of conductivities of ZMeImI and mPEG16MeImI. The curves represent VFT fits. Data for mPEG16-MeImI are re-plotted from ref. 21.

Table 2 Comparison of conductivities of ILs with block oligomer and homopolymer tails

	Conductivity (mS cm^{-1})		
IL	25 °C	85 °C	95 °C
ZMeImI (**1a**)	0.012	0.54	0.76
ZMeImTf$_2$N (**1b**)	0.12	1.67	2.17
mPEG7MeImI (**2a**)[a]	0.128	2.67	3.47
mPEG12MeImI (**2b**)[a]	0.119	2.15	2.70
mPEG16MeImI (**2c**)[a]	0.112	1.75	2.27

[a] Data from ref. 21.

ion-conducting PEGylated channels of relatively low viscosity within the ionogel. The low viscosity of the PEGylated channels (compared to ILs with non-polar tails, *e.g.*, 1-hexyl-3-methylimidazolium iodide) is because of H-bonding intramolecular interactions of the PEG segments with the imidazolium rings, weakening the Coulombic interactions between the imidazolium cation and the iodide anion.[21]

3.4. Effect of LiI and EtMeImI addition on ionic conductivity

One approach to further increasing the ionic conductivity of the ZMeImI based electrolytes is to dissolve salts such as LiI that will increase the concentration of ions in the material. Inorganic salts have been added to ILs in other previous studies.[38,39] Fig. 8 shows the effect of LiI mole fraction on the conductivity of ZMeImI ionogels. It is seen that the conductivities of the ZMeImI/LiI blends are actually lower than those of the pure ZMeImI. The decrease in conductivity is attributed to an increase in the viscosity of the PEGylated microdomains because of LiI. Takada *et al.* found that the viscosity of 1-butyl-3-methylimidazolium chloride increased with the addition of an inorganic salt, LiCl, and attributed the increase in viscosity to structure formation in the blend.[40] Thus, inorganic salts such as LiI may function as gelators for ILs, but they may not always result in the desired increase in conductivity. Hence, we considered the use of an organic salt such as EtMeImI to increase ionic conductivity.

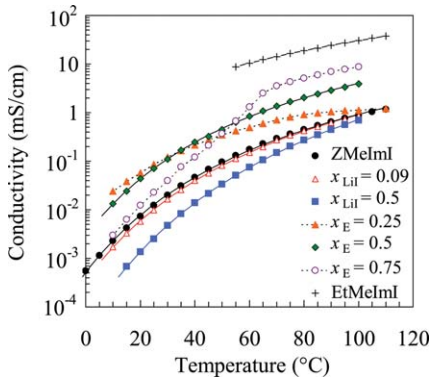

Fig. 8 Conductivity *vs.* temperature for (a) ZMeImI, (b) ZMeImI/LiI blends with LiI mole fractions, $x_{LiI} = 0.09$ and 0.5, (c) ZMeImI/EtMeImI blends with EtMeImI mole fractions, $x_E = 0.25$, 0.5 and 0.75, and (d) EtMeImI. The solid curves represent the VFT fits of the experimental data, and the dotted curves are drawn as guide for the eye. Data for EtMeImI are re-plotted from ref. 21.

1-Ethyl-3-methylimidazolium iodide is a crystalline solid at room temperature with a melting point of about 81.5 °C. Its conductivity is fairly high, in the range of 10 to 40 mS cm^{-1}, at temperatures between 60 and 110 °C (*cf.* Fig. 8). At these temperatures, the ionic conductivity of EtMeImI is higher than that of any of the other 1,3-dialkylimidazolium iodides that we studied, and is also higher than those of the mPEG*n*MeImI ILs.[21] While EtMeImI alone is difficult to use in a DSSC because of its crystalline powder-like form, it could be blended with ZMeImI to obtain an electrolyte with low-fluidity, similar to pure ZMeImI. Fig. 8 shows that, unlike LiI, EtMeImI generally resulted in an increase in the conductivity of ZMeImI for all mole fractions of EtMeImI in the blend. A clear increase in conductivity, throughout the temperature range of measurements, was observed for the mole fraction of EtMeImI in the blend, x_E, equal to 0.5. It should be noted that Bai *et al.*[41] have successfully used blends containing EtMeImI in DSSCs, but these blends were low melting eutectics with a melting point of 0 °C (and hence, liquids at room temperature). In contrast, the blends of the present study are hard-gels at room temperature.

Fig. 8 shows a discontinuous change in conductivity at about 65 °C when x_E is 0.75. A similar discontinuous increase in conductivity is observed at 60 °C in pure EtMeImI, which indicates the presence of crystallites of EtMeImI in the blend with $x_E = 0.75$. DSC was used to determine the extent of crystallinity of EtMeImI in the blends. Pure ZMeImI was found to be an amorphous material with a low glass transition temperature (T_g) of about −38 °C, whereas pure EtMeImI was a crystalline solid with a melting point of about 81.5 °C (Fig. 9). Therefore, the non-appearance of melting or crystallization peaks in the thermal analysis curves was considered as an indication of complete solvation of EtMeImI by ZMeImI. The ZMeImI/EtMeImI blend with $x_E = 0.75$ showed a distinct melting peak in the DSC curve (Fig. 9c). Using the enthalpy of melting of pure EtMeImI (74 J g^{-1}) and the mass fraction of EtMeImI in the blend (about 0.44),

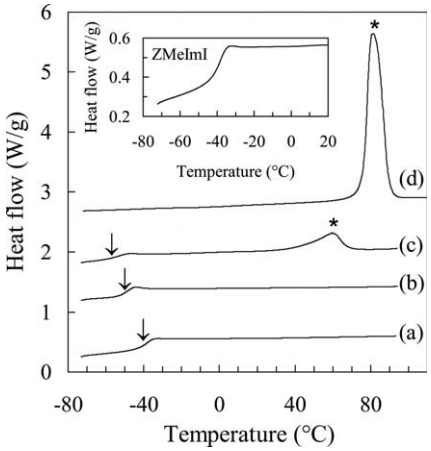

Fig. 9 DSC thermal analysis curves for ZMeImI (a), blends of ZMeImI and EtMeImI, $x_E = 0.56$ and 0.75 (b and c, respectively), and EtMeImI (d); nitrogen atmosphere and 20 °C min^{-1} heating rate. The DSC curves are vertically offset for clarity. Data for EtMeImI are re-plotted from ref. 21. Arrow denotes glass transition and * denotes EtMeImI melting transition. A melting point depression[43] is observed for EtMeImI, because of ZMeImI.

the degree of crystallinity of EtMeImI in the blend was calculated to be about 39%. Because of the incomplete dissolution of EtMeImI in the blend with $x_E = 0.75$, the conductivity enhancement was lower compared to blends with a lower mole fraction of EtMeImI ($x_E = 0.5$ or 0.25). No melting or crystallization peaks were observed for $x_E \leq 0.56$ (*cf.* Fig. 9b). Hence, below $x_E = 0.56$, EtMeImI was completely "solvated" by ZMeImI. Note that the absence of liquid crystalline mesophase transitions (which are expected for perfluoroalkyl segments longer than 6 carbon atoms[42]) in the DSC curves is attributed to the high degree of polydispersity in tail lengths.

As evident from Table 3, the concentration of iodide anion is significantly different in the five blends. This difference is partly responsible for the large differences in conductivities observed in Fig. 8. To account for the variations in I^- concentrations in the electrolytes, the conductivities were normalized by the I^- concentration. The normalized conductivity *vs.* temperature plots (data not shown) exhibited almost the same trend as conductivity *vs.* temperature plots in Fig. 8. Hence, differences in I^- concentrations alone cannot explain the variations in ionic conductivities of the ZMeImI blends. Clearly, the diffusion coefficient of cations is expected to be quite different for EtMeImI, ZMeImI, and LiI. Furthermore, microstructural differences could also be a factor, as discussed in the following section.

3.5. Self-consistent field modeling of microphase separation in ZMeImI and ZMeImI/EtMeImI blends

Microphase separation in ZMeImI was investigated using the Schuetjens and Fleer lattice model of the SCMF theory,[22,23] which has been widely used for modeling equilibrium phase behavior of structured polymer melts,[44–47] and recently for studying interfacial structure of ILs in electrical double-layer capacitors.[26] Early applications of this technique were focused on polymer films in which spatial variations in composition were limited to the direction normal to the film surface. More recently, the technique has been generalized to include spatial gradients in two directions, as in the case of side-chain semifluorinated polymers.[47]

ZMeImI is composed of a mixture of diblock molecules consisting of a perfluoroalkyl segment and a PEG segment, with a methylimidazolium head group that is connected to the PEG segment (*cf.* Fig. 1). It also contains free iodide anions. The ω-perfluoroalkyl PEG tails are of different lengths because the Zonyl® FSO-100 surfactant, $F(CF_2CF_2)_y(CH_2CH_2O)_xCH_2CH_2OH$, that is used in the synthesis of ZMeImI is quite polydisperse.[48–50] Using MALDI-TOF mass spectrometry,[48] and NMR spectroscopy (^1H and ^{19}F), the average values of x and y were estimated to be 6.8 and 3.6, respectively. The mass distribution obtained using MALDI-TOF spectrometry indicated that about 50 mol% of the surfactant consists of species with y = 5 (and x = 3, 4, 5, or 6; mean x = 4.2), and the remaining 50 mol% consisted of species with y = 2 (and x = 6, 7, 8, 9, 10, 11 or 12; mean x = 9.2).

From the experimental densities of a series of perfluoroalkanes and PEGs, the volumes occupied by the CF_2 and CH_2CH_2O groups were estimated to be 56 and 63 Å^3, respectively. The 1-ethyl-3-methylimidazolium cation and the iodide anion were estimated to occupy volumes of about 188 and 72 Å^3, respectively. Hence, the ZMeIm cation was represented by 7 CF_2 groups, 7 CH_2CH_2O groups, and an 1-ethyl-3-methylimidazolium head group. The aromatic head group was modeled as a linear segment consisting of 2 uncharged but polar "mers" and one charged "mer". This model was motivated by the fact that the volume of the imdazolium head group is roughly three times those of the CF_2 and CH_2CH_2O groups. Thus, the cations were considered to have a mer composition expressed by the empirical formula $H_1CAT_1H_1EO_xFM_{2y}$, where H represents an uncharged portion of the imidazolium cation, CAT represents the section of the imidazolium ring that carries the positive charge, EO denotes ethylene oxide (CH_2CH_2O), and FM denotes the perfluoromethylene (CF_2) group (and also the terminal CF_3 group). It was further assumed that the electrolyte contained a certain number of EtMeImI molecules (equal to 0 for pure ZMeImI), the cationic parts of which were represented by $H_1CAT_1H_1$. The iodide anions served to maintain electrical neutrality for the liquid as a whole.

Following van de Grampel,[47] a small amount of void space ($\varphi \cong 0.05$) was included in all of the simulations. The results of the simulations were found to be insensitive to small variations in void space around this value. Finally, as a boundary condition, it was assumed that the electrolyte "thin film" was in contact with vacuum on both sides. The X axis of the coordinate system was assumed to be perpendicular to the thickness of the film ($X = 0$ corresponding to mid-section of the film thickness), and the Y and Z axes were assumed to be in the plane of the film (*cf.* Fig. S9 of ESI†). In principle, $\chi_{FM,V}$ or $\chi_{EO,V}$, the interaction parameters between mers and the voids (which are also treated like mers and are denoted by "V"), can be estimated using the experimental surface tension and density of a perfluoroalkane or PEG, and the surface tension predicted by compressible lattice simulations.[51] In the present study, the interaction parameters between voids and all polar mers (EO, H, CAT, and iodide) were assumed to be equal to 2.0, whereas $\chi_{FM,V}$ was assumed to be equal to 1.2, consistent with the lower surface energy of fluoroalkyl moieties. The values of all interaction parameters were assumed to be independent of composition.

The relative permittivities of the H, CAT, EO, FM, and iodide mers were assumed to be 7, 25, 7, 2.1, and 25, respectively.[52,53] These values result in relative permittivities of 16 for EtMeImI and about 7.1 for ZMeImI, which are reasonable based on

Table 3 Molar concentration of iodide per unit mass of the blends of ZMeImI with LiI or EtMeImI

			LiI blends		EtMeImI blends		
	ZMeImI	EtMeImI	$x_{LiI} = 0.09$	$x_{LiI} = 0.5$	$x_E = 0.25$	$x_E = 0.5$	$x_E = 0.75$
Iodide conc. (mmol g^{-1})	1.092	4.200	1.184	1.905	1.340	1.733	2.454

microwave dielectric spectroscopy studies of ILs.[54] The simulations were performed for a three-dimensional lattice, but gradients were assumed in only one or two spatial directions. For this reason, only lamellar and hexagonal cylindrical microphases were obtained from the simulations. The coordination number used in most of the simulations was 6 (simple cubic), but simulations were also performed for tetrahedral coordination. The choice of cubic or tetrahedral coordination was not found to affect the shape of the observed microstructures.

Fig. 10 shows the volume fractions of FM, EO, $H_1CAT_1H_1$, and iodide mers in a film of pure ZMeImI, at different lattice cells along a normal to the plane of the film. The simulation was conducted using a lattice with 90 cells, assuming composition gradients only along the film thickness. The film was found to exhibit lamellar microstructures parallel to the electrolyte–vacuum interface ($X = \pm 90$). From the volume fraction profiles for the different mers, it is clear that the polar EO mers, the cations, and the anions (*cf.* curves b, c, and d in Fig. 10) were excluded from the regions occupied by the non-polar FM mers (*cf.* curve a in Fig. 10).

Fig. 11 shows a periodogram for the FM concentration profile shown in Fig. 10. The power values were calculated as squares of the magnitudes of the discrete Fourier transforms of φ_{FM} *vs.* X. The peak at frequency of 0.125 in the power spectrum corresponds to a lamellar d-spacing of 31.3 Å (corresponding to a dimensionless wavelength, ΔX, of 8).

For simulations involving composition gradients not only along the film thickness (X axis) but also along the length of the film (Y axis) (*cf.* Fig. S9 in ESI), additional simplifications were required for numerical computations. The polydispersity in the segment lengths of the ω-perfluoroalkyl PEG tails was ignored, and ZMeImI was modeled by a single block oligomer chain having a composition that was representative of the average composition of the tails (x ≈ 7, y ≈ 3.5). The power spectrum density of the lamellar composition profile for this average chain resulted in a d-spacing of 25.0 Å ($\Delta X \approx 6.4$), which is somewhat lower than the d-spacing of 31.3 Å obtained when the polydispersity was incorporated in the simulations, as expected. However, this difference was not expected to influence the primary conclusions drawn from the simulations considering the "average" ZMeImI molecule.

Pure ZMeImI was found to have a lamellar microstructure. However, SCMF theory predicted cylindrical microstructures for blends of EtMeImI and ZMeImI beyond a certain mole fraction of EtMeImI in the blend. The transition from lamellar to cylindrical microstructure was found to occur at an EtMeImI/ZMeImI ratio between 1.2 and 1.4 (that is for x_E between 0.55

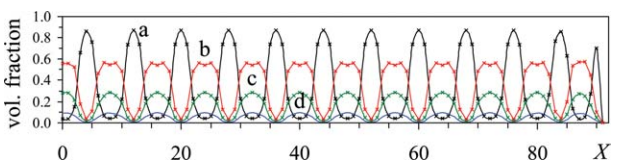

Fig. 10 Volume fractions of (a) FM, (b) EO, (c) $H_1CAT_1H_1$ and (d) iodide in different layers parallel to the plane of the ZMeImI film. Abscissas are distances of the centers of these layers from the origin ($X = 0$), non-dimensionalized using the length of the cubic lattice cell (3.9 Å). The film-vacuum interfaces are at $X = \pm 90$.

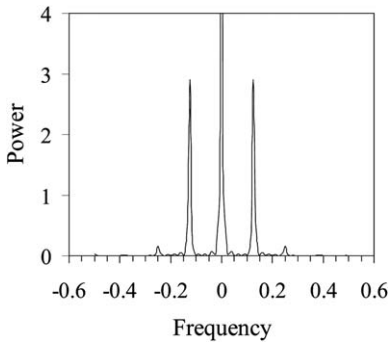

Fig. 11 Periodograms for CF_2 density distribution in ZMeImI.

and 0.58). Interestingly, $x_E \approx 0.56$ was also the composition threshold above which melting peaks were observed in the DSC analysis (*cf.* Fig. 9), which implies that the change in microstructure that occurs beyond this composition results in better packing of the imidazolium rings in the blend and imparts partial crystallinity to the cationic head groups.

Fig. 12a–d show the contour plots for density distributions of the iodide anions, the 1-ethyl-3-methylimidazolium cations, and the FM and EO mers in blends containing EtMeImI and ZMeImI in a mole ratio of 3 : 1 (that is, $x_E = 0.75$). Cylindrical microdomains (with cylinder axes oriented along the Z axis) are clearly evident from these plots. In thin films of this blend, the PEG segments, the cations, and the anions constitute the continuous phase (Fig. 12a–c). Hence, the iodide ions would have a continuous path to diffuse through the PEG matrix. One might, therefore, expect that the electrical conductivity of the blend would be higher than that of pure ZMeImI with a paracrystalline lamellar microstructure. The higher conductivity of the blend (with $x_E = 0.75$) compared to pure ZMeImI, as shown in Fig. 8, is attributed to: (i) an increase in the concentration of ions in the blend (*cf.* Table 3), and (ii) a change in the microstructure from lamellar, in pure ZMeImI, to cylindrical, in the EtMeImI/ZMeImI blend.[55,56] Both lamellar and cylindrical morphologies are expected to result in higher viscosities than unstructured fluids because of the presence of large molecular aggregates in the fluid.

In Fig. 12, the right edge of each box corresponds to the electrolyte-vacuum interface. The iodide and imidazolium ions, and the EO mers are excluded from this interface because of preferential surface segregation of the low surface-energy fluoroalkyl groups. The stoichiometric volume fraction of iodide in the blend with $x_E = 0.75$ is 4/30 (≈0.133). However, as seen in Fig. 12a, there is non-uniform distribution of iodide in the lattice, and φ_{iodide} ranges from 0 to 0.16. The lattice sites where $\varphi_{iodide} \approx 0$ are occupied by the FM mers. The iodide anions and the cationic head groups are dispersed within the PEGylated microdomains, and are excluded from the cores of the non-polar fluoroalkyl domains.

Fig. 12b shows localized spots of relatively high EtMeIm cation concentration ($\varphi_{cation} \approx 0.50$) at sites that are farthest from the axis of the fluoroalkyl cylindrical microdomains. These spots are most likely similar to the ionic clusters that have been previously observed in other systems such as halato-telechelic homopolymers.[33,34] The volume fraction of EO mers is correspondingly low at these sites. Fig. 12c shows the distribution of

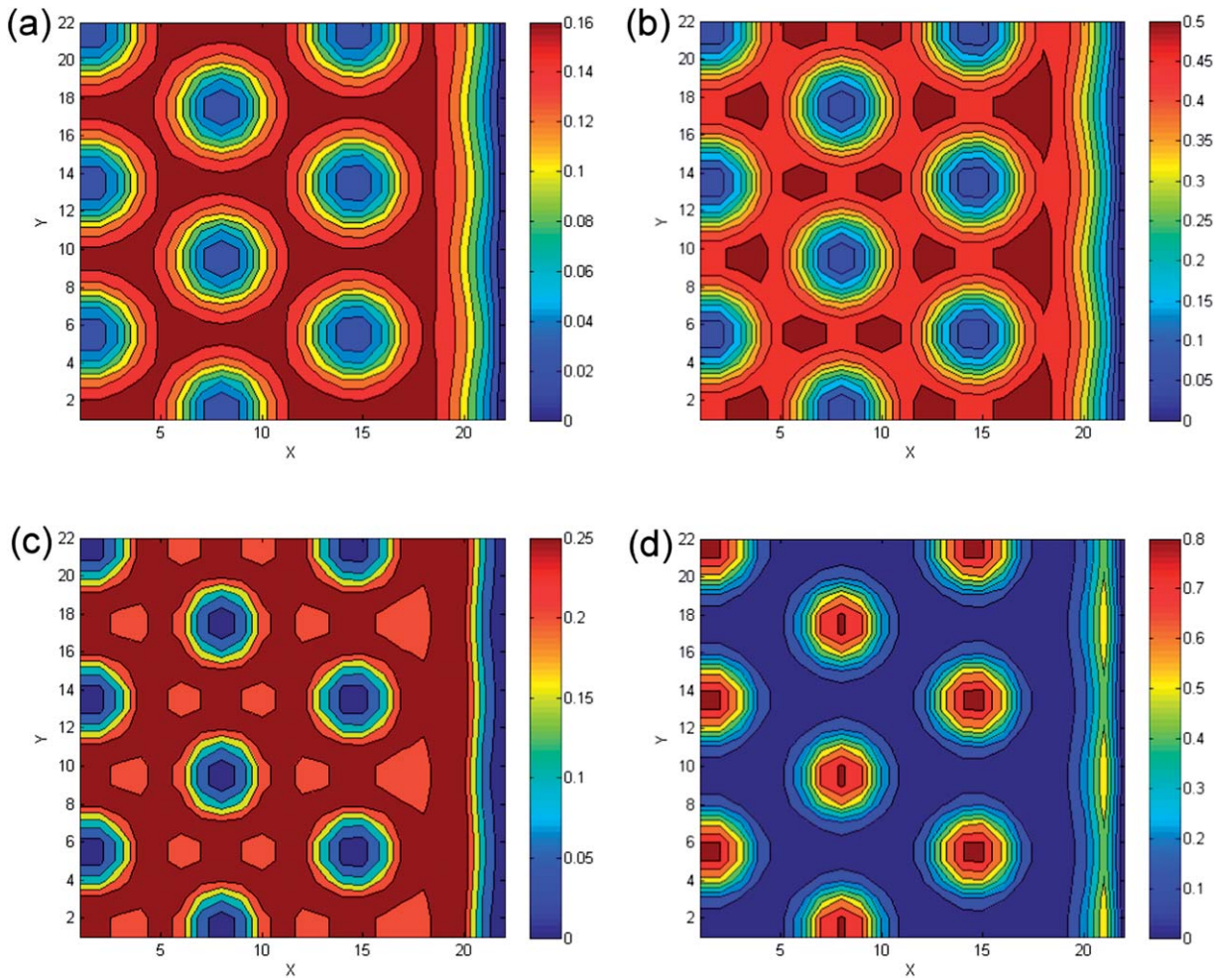

Fig. 12 Volume fractions of (a) iodide, (b) the cations, $H_1CAT_1H_1$, (c) the EO mers, and (d) the FM mers for an electrolyte blend in which the molar ratio of EtMeImI to ZMeImI is 3 ($x_E = 0.75$). The width of each box is about 86 Å.

EO mers. The stoichiometric volume fraction of EO in the blend is 7/30 ($\approx$0.233). However, the actual volume fraction varies between 0 and 0.25. The density distribution of the FM mers are shown in Fig. 12d. Although the stoichiometric volume fraction of these mers is about 0.233, the FM mers are almost completely excluded from other polar mers and form cylindrical nanodomains with φ_{FM} as high as 0.80.

The regions of high EtMeIm cation concentration (Fig. 12b) are most likely the spots where EtMeImI would be present in the crystalline form (see discussion related to Fig. 9). Note that our simulations did not explicitly take into account crystallization in the blends. Crystallization is expected to affect the values of the interaction parameter and void fractions in the blend, but incorporation of these details in the simulation is beyond the scope of our study.

4. Conclusions

Novel block oligomer ILs have been synthesized and the experimentally observed transport properties have been rationalized on the basis of the microstructure formation predicted by SCMF theory. The electrostatic interactions between the imidazolium cation and the iodide anion in the IL, intermolecular van der Waals interactions between the block copolymer tails, and microphase separation because of the immiscibility of the PEG and fluoroalkyl segments result in spontaneous self-assembly of the IL molecules to form thermoreversible solvent-free ionic gels.

To prevent leakage from the photovoltaic devices, it is necessary that the electrolytes have large viscosities. At the same time, high ionic conductivity is necessary for satisfactory device performance. Although these properties appear incompatible, we have shown that by using an optimized blend of two components (ZMeImI and EtMeImI) that are solids at room temperature, nanostructured ionogels which exhibit large effective viscosities and high ionic conductivities can be obtained.

Ionic conductivity in the ionogels is controlled by the concentrations of free cations and iodide ions, and also by the relative sizes (and hence the diffusion coefficients) of these ions. Moreover, electrostatic interactions and miscibility of different groups in the IL play a strong role in influencing its fluidity. When the iodide ions in the ω-perfluoroalkyl PEG functionalized imidazolium salt were replaced by the bistriflimide (Tf_2N) anions, an IL with a relatively low viscosity was obtained. Weaker electrostatic interactions, because of charge delocalization in the bulkier Tf_2N anion, and partial miscibility of the fluorinated anion with the fluoroalkyl tail of the cation are

possible reasons for this behavior. A detailed investigation of these effects will be a topic of future study.

Acknowledgements

We would like to thank Professor Frans Leermakers for his help with the *sfbox* program, and Ms Janice Lebga for her assistance with some of the viscosity measurements.

Notes and references

1 J. Le Bideau, L. Viau and A. Vioux, *Chem. Soc. Rev.*, 2011, **40**, 907–925.
2 J. Wu, Z. Lan, S. Hao, P. Li, J. Lin, M. Huang, L. Fang and Y. Huang, *Pure Appl. Chem.*, 2008, **80**, 2241–2258.
3 Y. Wang, *Sol. Energy Mater. Sol. Cells*, 2009, **93**, 1167–1175.
4 J. Zhao, X. Shen, F. Yan, L. Qiu, S. Lee and B. Sun, *J. Mater. Chem.*, 2011, **21**, 7326–7330.
5 C.-H. Lee, W.-H. Chiu, K.-M. Lee, W.-F. Hsieh and J.-M. Wu, *J. Mater. Chem.*, 2011, **21**, 5114–5119.
6 A. D. Pasquier, *Electrochim. Acta*, 2007, **52**, 7469–7474.
7 C. Longo, A. F. Nogueira, M.-A. De Paoli and H. Cachet, *J. Phys. Chem. B*, 2002, **106**, 5925–5930.
8 P. C. Trulove and R. A. Mantz, in *Ionic Liquids in Synthesis, Volume 1*, ed. P. Wasserscheid and T. Welton, Wiley-VCH, Weinheim, 2008, ch. 3.6, pp. 141–174.
9 W. Kubo, T. Kitamura, K. Hanabusa, Y. Wada and S. Yanagida, *Chem. Commun.*, 2002, 374–375.
10 W. Kubo, S. Kambe, S. Nakade, T. Kitamura, K. Hanabusa, Y. Wada and S. Yanagida, *J. Phys. Chem. B*, 2003, **107**, 4374–4381.
11 N. Mohmeyer, D. Kuang, P. Wang, H.-W. Schmidt, S. M. Zakeeruddin and M. Grätzel, *J. Mater. Chem.*, 2006, **16**, 2978–2983.
12 N. Mohmeyer, P. Wang, H.-W. Schmidt, S. M. Zakeeruddin and M. Grätzel, *J. Mater. Chem.*, 2004, **14**, 1905–1909.
13 F. S. Freitas, J. N. de Freitas, B. I. Ito, M. A. D. Paoli and A. F. Nogueira, *ACS Appl. Mater. Interfaces*, 2009, **1**, 2870–2877.
14 P. K. Singh, K.-I. Kim, N.-G. Park and H.-W. Rhee, *Macromol. Symp.*, 2007, **249–250**, 162–166.
15 P. K. Singh, K.-W. Kim and H.-W. Rhee, *Synth. Met.*, 2009, **159**, 1538–1541.
16 P. Wang, S. M. Zakeeruddin, J. E. Moser, M. K. Nazeeruddin, T. Sekiguchi and M. Grätzel, *Nat. Mater.*, 2003, **2**, 402–407.
17 P. Wang, S. M. Zakeeruddin, I. Exnar and M. Grätzel, *Chem. Commun.*, 2002, 2972–2973.
18 Y. Yang, J. Zhang, C. Zhou, S. Wu, S. Xu, W. Liu, H. Han, B. Chen and X.-Z. Zhao, *J. Phys. Chem. B*, 2008, **112**, 6594–6602.
19 Y. He, P. G. Boswell, P. Bühlmann and T. P. Lodge, *J. Phys. Chem. B*, 2007, **111**, 4645–4652.
20 J. Lee, M. J. Panzer, Y. He, T. P. Lodge and C. D. Frisbie, *J. Am. Chem. Soc.*, 2007, **129**, 4532–4533.
21 L. V. N. R. Ganapatibhotla, J. Zheng, D. Roy and S. Krishnan, *Chem. Mater.*, 2010, **22**, 6347–6360.
22 J. M. H. M. Scheutjens and G. J. Fleer, *J. Phys. Chem.*, 1979, **83**, 1619–1635.
23 J. M. H. M. Scheutjens and G. J. Fleer, *J. Phys. Chem.*, 1980, **84**, 178–190.
24 J. van Male, Ph.D. Thesis, The University of Wageningen, The Netherlands, 2003.
25 R. G. Larson, in *The Structure and Rheology of Complex Fluids*, Oxford University Press, New York, 1999, ch. 2, pp. 61–104.
26 Y. Lauw, M. D. Horne, T. Rodopoulos, A. Nelson and F. A. M. Leermakers, *J. Phys. Chem. B*, 2010, **114**, 11149–11154.
27 A. Kelarakis, W. Mingvanish, C. Daniel, H. Li, V. Havredaki, C. Booth, I. W. Hamley and A. J. Ryan, *Phys. Chem. Chem. Phys.*, 2000, **2**, 2755–2763.
28 J. H. Park, K. J. Choi, J. Kim, Y. S. Kang and S.-S. Lee, *J. Power Sources*, 2007, **173**, 1029–1033.
29 J. M. Sebastian, C. Lai, W. W. Graessley, R. A. Register and G. R. Marchand, *Macromolecules*, 2002, **35**, 2700–2706.
30 D. L. Polis, K. I. Winey, A. J. Ryan and S. D. Smith, *Phys. Rev. Lett.*, 1999, **83**, 2861–2864.
31 Y. G. Jeong, N. V. Pagodina, C. Jiang, S. L. Hsu and C. W. Paul, *Macromolecules*, 2006, **39**, 4907–4913.
32 E. B. Christiansen, N. W. Ryan and W. E. Stevens, *AIChE J.*, 1955, **1**, 544–548.
33 M. Goswami, S. K. Kumar, A. Bhattacharya and J. F. Douglas, *Macromolecules*, 2007, **40**, 4113–4118.
34 C. E. Williams, T. P. Russell, R. Jerome and J. Horrion, *Macromolecules*, 1986, **19**, 2877–2884.
35 J. R. Macdonald, *Solid State Ionics*, 1984, **13**, 147–149.
36 J. P. Zheng, P. C. Goonetilleke, C. M. Pettit and D. Roy, *Talanta*, 2010, **81**, 1045–1055.
37 C. A. C. Sequeira, M. J. C. Plancha and L. P. S. Araújo, *J. Phys. IV France*, 1994, **4**, C1-17–C1-35.
38 Y. Wang, Y. Sun, B. Song and J. Xi, *Sol. Energy Mater. Sol. Cells*, 2008, **92**, 660–666.
39 S. R. Kim, M. K. Parvez, I. In, H. Y. Lee and J. M. Park, *Electrochim. Acta*, 2009, **54**, 6306–6311.
40 A. Takada, K. Imaichi, T. Kagawa and Y. Takahashi, *J. Phys. Chem. B*, 2008, **112**, 9660–9662.
41 Y. Bai, Y. Cao, J. Zhang, M. Wang, R. Li, P. Wang, S. M. Zakeeruddin and M. Grätzel, *Nat. Mater.*, 2008, **7**, 626–630.
42 S. Krishnan, Y.-J. Kwark and C. K. Ober, *Chem. Rec.*, 2004, **4**, 315–330.
43 S. D. Rostami, *Eur. Polym. J.*, 2000, **36**, 2285–2290.
44 M. W. Matsen, in *Soft Matter*, Wiley-VCH Verlag GmbH & Co. KGaA, 2007, pp. 87–178.
45 M. Müller, in *Modeling and Simulation in Polymers*, Wiley-VCH Verlag GmbH & Co. KGaA, 2010, pp. 197–246.
46 O. A. Evers, J. M. H. M. Scheutjens and G. J. Fleer, *Macromolecules*, 1990, **23**, 5221–5233.
47 R. D. van de Grampel, W. Ming, J. Laven, R. van der Linde and F. A. M. Leermakers, *Polymer*, 2007, **48**, 3877–3882.
48 S. Krishnan, R. Ayothi, A. Hexemer, J. A. Finlay, K. E. Sohn, R. Perry, C. K. Ober, E. J. Kramer, M. E. Callow, J. A. Callow and D. A. Fischer, *Langmuir*, 2006, **22**, 5075–5086.
49 J. L. Fulton, D. M. Pfund, J. B. McClain, T. J. Romack, E. E. Maury, J. R. Combes, E. T. Samulski, J. M. DeSimone and M. Capel, *Langmuir*, 1995, **11**, 4241–4249.
50 M. Lísal, C. K. Hall, K. E. Gubbins and A. Z. Panagiotopoulos, *J. Chem. Phys.*, 2002, **116**, 1171–1184.
51 V. S. Minnikanti and L. A. Archer, *Macromolecules*, 2006, **39**, 7718–7728.
52 The relative permittivity of tetraethylene glycol dimethyl ether is 7.68, of perfluorohexane is 1.76, and of polytetrafluoroethylene is 2.1 at 25 °C. See ref. 53.
53 Permittivity (Dielectric Constant) of Liquids, in *CRC Handbook of Chemistry and Physics*, 92nd Edition (Internet Version 2012), ed. W. M. Haynes, CRC Press/Taylor and Francis, Boca Raton, FL.
54 C. Wakai, A. Oleinikova, M. Ott and H. Weingärtner, *J. Phys. Chem. B*, 2005, **109**, 17028–17030.
55 Disko *et al.*, however, reported that shearing of a lamellar microstructure can lead to a persistent catenoid lamellar microstructure in which one of the phases become continuous. Such a microstructure formation is possible in ZMeImI when the ionogel is loaded in the conductivity cell for measurements.
56 M. M. Disko, K. S. Liang, S. K. Behal, R. J. Roe and K. J. Jeon, *Macromolecules*, 1993, **26**, 2983–2986.